J. Membrane Biol. 199, 143–154 (2004)
DOI: 10.1007/s00232-004-0682-y

The Journal of
Membrane
Biology

Conductive and Kinetic Properties of Connexin45 Hemichannels Expressed in Transfected HeLa Cells

P. Bader, R. Weingart
Department of Physiology, University of Bern, CH-3012, Bern, Switzerland

Received: 12 November 2003/Revised: 2 April 2004

Abstract. Human HeLa cells transfected with mouse connexin Cx45 were used to examine the conductive and kinetic properties of Cx45 hemichannels. The experiments were carried out on single cells using a voltage-clamp method. Lowering the $[Ca^{2+}]_o$ revealed an extra current. Its sensitivity to extracellular Ca^{2+} and gap junction channel blockers (18α-glycyrrhetinic acid, palmitoleic acid, heptanol), and its absence in non-transfected HeLa cells suggested that it is carried by Cx45 hemichannels. The conductive and kinetic properties of this current, I_{hc}, were determined adopting a biphasic pulse protocol. I_{hc} activated at positive V_m and deactivated partially at negative V_m. The analysis of the instantaneous I_{hc} yielded a linear function $g_{hc,inst} = f(V_m)$ with a hint of a negative slope ($g_{hc,inst}$: instantaneous conductance). The analysis of the steady-state I_{hc} revealed a sigmoidal function $g_{hc,ss} = f(V_m)$ best described with the Boltzmann equation: $V_{m,0} = -1.08$ mV, $g_{hc,min} = 0.08$ ($g_{hc,ss}$: steady-state conductance; $V_{m,0}$: V_m at which $g_{hc,ss}$ is half-maximally activated; $g_{hc,min}$: minimal conductance; major charge carriers: K^+ and Cl^-). The g_{hc} was minimal at negative V_m and maximal at positive V_m. This suggests that Cx45 connexons integrated in gap junction channels are gating with negative voltage. I_{hc} deactivated exponentially with time, giving rise to single time constants, τ_d. The function $\tau_d = f(V_m)$ was exponential and increased with positive V_m ($\tau_d = 7.6$ s at $V_m = 0$ mV). The activation of I_{hc} followed the sum of two exponentials giving rise to the time constants, τ_{a1} and τ_{a2}. The function $\tau_{a1} = f(V_m)$ and $\tau_{a2} = f(V_m)$ were bell-shaped and yielded a maximum of $\cong 0.6$ s at $V_m \cong -20$ mV and $\cong 4.9$ s at $V_m \cong 15$ mV, respectively. Neither $\tau_{a1} = f(V_m)$ nor $\tau_{a2} = f(V_m)$ coincided with $\tau_d = f(V_m)$. These findings conflict with the notion that activation and deactivation follow a simple reversible reaction scheme governed by first-order voltage-dependent processes.

Key words: Gap junction hemichannel — Connexin45 — Conductance — Kinetics — Electrophysiology — Heart

Introduction

Gap junction channels provide a direct pathway for the exchange of mediators of intercellular signaling. They consist of two hemichannels or connexons arranged in series. Each connexon contains 6 subunits or connexins forming an aqueous pore sufficiently large to accommodate ions or small molecules. Connexins are integral membrane proteins that span the membrane four times, thus forming four transmembrane domains (M1–M4), two extracellular loops (E1, E2), a cytoplasmic loop (CL) and an intracellular amino (NT) and carboxyl tail (CT). So far, 19 different connexins have been identified in the mouse genome and 20 in the human genome (*cf.* Willecke et al., 2002). Connexins are transcripts of a multi-gene family.

The trafficking and assembly of connexins into gap junction channels have been investigated extensively (Martin et al., 2001). There is evidence for the coexistence of two parallel pathways. The classical route involves oligomerization of connexins into hexamers in the Golgi apparatus and subsequent transport to the plasma membrane; an alternative route involves initiation of oligomerization in the ER and transport to the plasma membrane bypassing the Golgi. Both concepts suggest that hemichannels are already present in the plasma membrane of single cells. This is consistent with the results from experiments examining the de novo formation of gap junction channels (Bukauskas and Weingart, 1994).

Cell-pair preparations have been widely used to study the electrical properties of gap junctions and

Correspondence to: R. Weingart; email: weingart@pyl.unibe.ch

gap junction channels (*cf.* Bruzzone White & Paul 1996). The parameters gained from these studies allowed the design of a mathematical model that describes the operation of the channels (Vogel & Weingart, 1998). More recently, it has been reported that gap junction hemichannels can be examined in cellular preparations using isolated primary cells (De Vries & Schwartz, 1992; Kondo et al., 2000), injected oocytes (Ebihara, Berthoud & Beyer, 1995; Trexler et al., 1996) or transfected cell lines (Li et al., 1996; Valiunas & Weingart, 2000; Valiunas, 2002).

The connexin Cx45 is prominently expressed in the cardiovascular system, primarily in the SA-node, the AV-node and the bundle branches (Gros & Jongsma, 1996; Severs et al., 2001). It has also been found in other tissues such as smooth muscle and neurons (*cf.* Willecke et al., 2002). The electrical properties of Cx45 gap junction channels have been studied by several laboratories. They exhibit a low unitary conductance and a high voltage sensitivity (Barrio et al., 1997; Van Veen et al., 2000; Elenes et al., 2001). More recently, Cx45 hemichannels have been used to explore the electrical and diffusional behavior (Valiunas, 2002).

The aim of this study was to determine the conductive and kinetic properties of Cx45 hemichannels at the multichannel level. To this end, we have used transfected HeLa cells expressing mouse Cx45 (mCx45 or mouse connexin α_6; molecular mass or Greek letter nomenclature, respectively; Butterweck et al., 1994; Elfgang et al., 1995). We have determined the instantaneous and steady-state I/V relationship and elucidated the voltage dependence of I_{hc} deactivation and activation. The data gained are relevant for the heart during tachycardia prevailing both during physiological and pathophysiological conditions. Preliminary data have been published elsewhere in abstract form (Bader & Weingart, 2003).

Materials and Methods

Cells and Culture Conditions

Transfected human HeLa cells expressing mouse connexin45, mCx45 (Butterweck et al., 1994; Elfgang et al., 1995), and non-transfected HeLa cells were grown in Dulbecco's medium (DMEM) containing 10% fetal calf serum (FCS), 100 μg/ml streptomycin and 100 U/ml penicillin (2212 Seromed; Fakola, Basel, Switzerland). Transfected cells were selected using 0.5-1 μM puromycin (P−7255; Sigma). For experiments, cells were harvested in DMEM with 10% FCS (~$0.2{\cdot}10^6$ to ~$1{\cdot}10^6$ cells/ml) and seeded onto sterile glass coverslips placed in multi-well culture dishes and used within 24 h after plating.

Solutions

Experiments were carried out in K^+-rich solution containing normal Ca^{2+} (in mM): KCl 140, NaCl 4, $CaCl_2$ 2, $MgCl_2$ 1, HEPES 5 (pH = 7.4), glucose 5, pyruvate 2, $CsCl_2$ 2, $BaCl_2$ 1, TEA^+-Cl^- 2; or K^+-rich solution containing a reduced [Ca^{2+}] (in mM): $CaCl_2$ 1, EGTA (ethylene glycol-bis(2aminoethyl)-N,N,N',N'-tetra-acetic acid) 10 (free Ca^{2+}: 7.6 nM corresponding to a pCa = 8.1). Patch pipettes were filled with regular pipette solution (in mM): KCl 140, NaCl 4, $CaCl_2$ 1, $MgCl_2$ 1, Mg-ATP 3, HEPES 5 (pH = 7.2), EGTA 5 (free Ca^{2+}: 43 nM, corresponding to pCa = 7.4), $CsCl_2$ 2, $BaCl_2$ 1, TEA-Cl 2. Ba^{2+}, Cs^+ and TEA^+ served to block the K^+ channels. Mibefradil (20 μM; a gift from Roche Pharma, Basel, Switzerland) was added to the extracellular solutions to block the volume-regulated Cl^- channels (Nilius et al., 1998; Bader & Weingart, unpublished results). 18α-glycyrrhetinic acid (G−8503; Sigma) and (palmitoleic acid (P−9417; Sigma) were dissolved in DMSO and hexane (10 mM stock solutions), respectively, before dilution into K^+-rich solution.

Electrical Measurements

Glass coverslips with adherent cells were transferred to a chamber superfused with Ca^{2+}-containing solution at room temperature (22–26°C). The chamber was mounted on the stage of an inverted microscope equipped with phase-contrast optics (Diaphot-TMD, Nikon; Nippon Kogaku, Tokyo, Japan). Patch pipettes were pulled from glass capillaries (GC150F−10; Harvard Apparatus, Edenbridge, UK) using a horizontal puller (DMZ-Universal; Zeitz Instruments, Munich, Germany). The tip of the pipettes was coated with a silicon elastomer to reduce the capacitance (Sylgard 184; Dow Corning, Wiesbaden, Germany). When filled with solution, the pipettes had DC resistances of 2–6 MΩ. Experiments were carried out on single cells using a single voltage-clamp method (Valiunas & Weingart, 2000). After selection of a cell, a gigaohm-seal was produced and the conditions for whole-cell recording were established. The patch pipette was fixed in a pipette holder mounted on a micromanipulator (MP−258; Sutter Instrument, Novato, USA) and connected to an amplifier (EPC 7; HEKA Elektronik, Darmstadt, Germany). The method permitted control of the membrane potential V_m, and measurement of the associated current, I_m.

Signal Recording and Analysis

For analysis, unless otherwise stated, the signals were filtered at 1 kHz (8-pole Bessel filter) and digitized at 3.33 kHz with an A/D converter (ITC−16, Instrutech, Port Washington, NY, USA). Data acquisition and analysis were done with the software Pulse/PulseFit (HEKA Elektronik). Curve fitting and statistical analysis were performed with SigmaPlot and SigmaStat, respectively (Jandel Scientific, Erkrath, Germany). The results are presented as means ± SEM.

Results

Recruitment of Hemichannels

Figure 1 illustrates the procedure used to open putative hemichannels. A HeLa cell expressing mCx45 was patched in the presence of K^+-rich solution with normal Ca^{2+} (2 mM). After establishing the whole-cell configuration, the membrane potential, V_m, was measured, being close to 0 mV, as expected for $[K^+]_o = [K^+]_i$. After activation of the voltage-clamp, a biphasic voltage pulse was applied every

30 s. Starting from a holding potential V_h = 0 mV, V_m was first depolarized to 30 mV for 10 s and then hyperpolarized to −40 mV for 5 s (Fig. 1*A*). At time t = 0 min, low-Ca^{2+} solution (7.6 nM) was washed in. Figure 1*B* shows 2 superimposed current traces, I_m, recorded during control and 3 min after the intervention. During control, I_m showed a small outward component of constant amplitude, followed by a small inward component of constant amplitude. In the presence of low $[Ca^{2+}]_o$, the depolarizing step was accompanied by a large outward component that increased with time, while the hyperpolarizing step was associated with a large inward component that decreased with time to a level different from the reference level.

Figure 1*C* illustrates the change of I_m during wash-in of low-Ca^{2+} solution. For this purpose, the amplitudes of the following current components were determined and plotted as a function of time: $I_{m,max}$ (max: maximal; Δ), $I_{m,inst}$ (*inst*: instantaneous; ○) and $I_{m,ss}$ (*ss*: steady state; ●), prevailing at the end of the depolarizing pulse, the beginning of the hyperpolarizing pulse and the end of the hyperpolarizing pulse, respectively. During wash-in of low-Ca^{2+} solution, $I_{m,max}$ and $I_{m,inst}$ increased from nearly zero to a substantial outward and inward current, respectively, while $I_{m,ss}$ increased only slightly. The similar time course of $I_{m,max}$, $I_{m,inst}$ and $I_{m,ss}$ is consistent with a sequential recruitment of hemichannel currents. At hyperpolarizing steps, $I_{m,ss}$ was always much smaller than $I_{m,inst}$. This is in agreement with a transition of hemichannels from a completely open state to a partially closed state. The latter is reminiscent of the residual state of gap junction channels. Upon return to Ca^{2+}-containing solution, the extra current components vanished (*data not shown*). This suggests that the hemichannels that had opened previously closed again. In fact, the small current components observed during the control period disappeared virtually completely. This means that the channels responsible for the initial background current were blocked and/or downregulated. Hence, an interference from these channels was negligible. In a given cell, the Ca^{2+}-sensitive extra current could be recruited repetitively and showed consistent properties.

To ascertain that the extra I_m is mediated by Cx45 hemichannels, the following control experiments were performed (*data not shown*). Examining Cx45-HeLa cells exposed to low-Ca^{2+} solution, we found that the extra I_m was reversibly blocked by the gap junction blockers 18α-glycyrrhetinic acid (40 μM), palmitoleic acid (40 μM) or heptanol (3 mM) (*cf.* Harris, 2001). Moreover, non-transfected HeLa cells exposed to low-Ca^{2+} solution failed to generate an extra I_m. These observations support the view that the Ca^{2+}-sensitive extra current is carried by Cx45 hemichannels. Hence, it was called hemichannel current, I_{hc}.

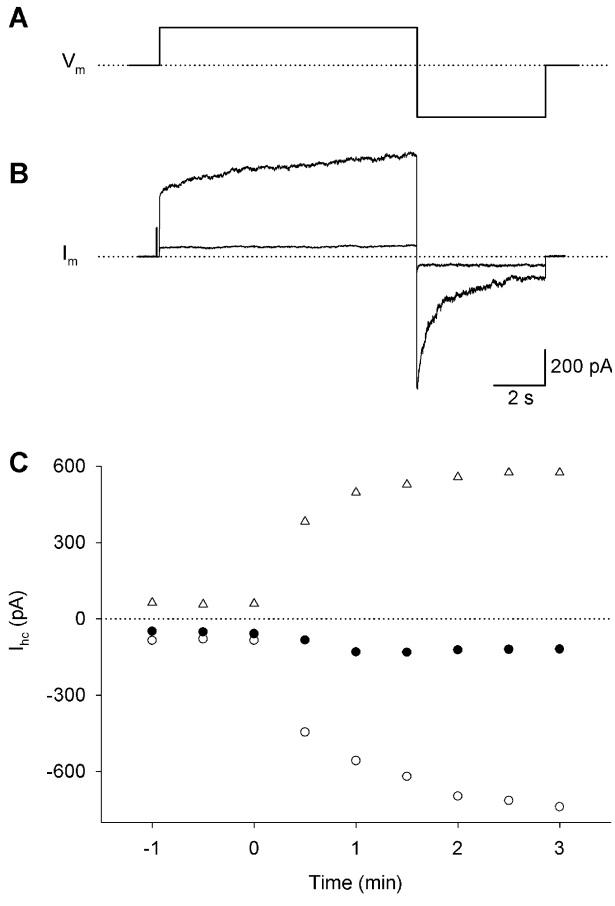

Fig. 1. Recruitment of hemichannel currents. (*A*) Biphasic voltage pulse to elicit currents carried by hemichannels. Starting from 0 mV, V_m was depolarized to 30 mV for 10 s and then hyperpolarized to −40 mV for 5 s. *Dotted line*: V_m = 0 mV. (*B*) Superimposed current traces I_m recorded in control solution (pCa_o = 2.7) and after wash-in of low-Ca^{2+} solution (pCa_o = 8.1) for 3 min. The intervention was started at time t = 0 min. The extra current components are attributable to hemichannels. The amplitude of I_m at the end of the depolarizing pulse corresponds to $I_{m,max}$ (max: maximal); the amplitude of I_m at the beginning and end of the hyperpolarizing pulse correspond to $I_{m,inst}$ (inst: instantaneous) and $I_{m,ss}$ (ss: steady state), respectively. The dotted line corresponds to the zero-current level. (*C*) Plot of current components as a function of time after exposure to low-Ca^{2+} solution. (Δ), $I_{m,max}$; (○), $I_{m,inst}$; (●), $I_{m,ss}$.

Voltage Dependence of Hemichannel Currents

Cells with operational hemichannels were then used to examine the voltage dependence of I_{hc}. This involved the biphasic pulse protocol consisting of a conditioning pulse followed by a test pulse. The conditioning pulse of constant amplitude activated the current, the test pulse of variable amplitude served to study the properties of I_{hc}. Preliminary experiments revealed that a conditioning pulse to 30 mV for 10 or 20 s fully activated I_{hc}. The subsequent test pulse was varied in amplitude and duration. It covered the voltage range between −50 and

60 mV, using increments of 5, 10 or 20 mV and lasted 7 to 20 s, depending on the time required for I_{hc} to reach a new steady-state level. The biphasic pulses were repeated at intervals long enough for I_{hc} to recover, i.e., 10 to 30 s, depending on V_m of the test pulse. V_h was again set to 0 mV.

Figure 2*A* shows the voltage protocol applied and Fig. 2*B*, the associated currents recorded. The conditioning pulse elicited an outward current. After a sudden rise, it increased gradually with time, approaching a steady state. The initial level reflects the current through the channels already in the main state plus the channels in the residual state at $V_m = 0$ mV; the quasi steady-state level reflects the current through all the channels in the main state. The subsequent test pulse yielded I_{hc} signals whose direction and contour was dependent on V_m. Hyperpolarization of V_m gave rise to inward currents with an instantaneous peak, $I_{hc,inst}$ followed by a decrease to a steady-state level, $I_{hc,ss}$ ($V_m = -50, -30, -15, -5$ mV). The latter was different from the holding current, suggesting an incomplete deactivation. The more negative V_m, the larger was the amplitude of $I_{hc,inst}$ and the faster the time course of decay. Depolarization of V_m led to outward currents with virtually no change in time ($V_m = 15$ mV) or a small time-dependent increase ($V_m = 40$ mV). The more positive V_m, the larger was the amplitude of $I_{hc,inst}$ and $I_{hc,ss}$.

For analysis, the amplitudes of $I_{hc,inst}$ and $I_{hc,ss}$ were determined for each test pulse. To account for spontaneous changes during an experimental run, the amplitude of $I_{hc,max}$ was used as reference. The values I_{hc} corrected in this way were plotted as a function of V_m, as shown in Fig. 3. Each symbol corresponds to a single determination. The function $I_{hc,inst} = f(V_m)$ (○) yielded a nearly constant slope. At the largest values of V_m, there was a tendency to deviate from linearity, i.e., the data points were bending towards the *x*-axis. In contrast, the function $I_{hc,ss} = f(V_m)$ (●) showed a prominent break around $V_m = 0$ mV. The data points at negative V_m were significantly smaller than those at positive V_m. While the latter yielded a quasi-linear relationship, the former did not.

The values $I_{hc,inst}$ and $I_{hc,ss}$ were then used to calculate the conductances $g_{hc,inst}$ and $g_{hc,ss}$, respectively. After normalization, the conductances gained from 8 cells were sampled, averaged and plotted as a function of V_m. In order to normalize the $g_{hc,inst}$ data, a value extrapolated to $V_m = 0$ mV was used as reference. It was obtained by averaging the values of $g_{hc,inst}$ at nearby voltages, i.e. ± 5 mV. In order to normalize the $g_{hc,ss}$ data, the values of $g_{hc,ss}$ from each cell were expressed as a fraction of $g_{hc,inst}$ prevailing during the same pulse. Figure 4*A* shows the plots of the function $g_{hc,inst} = f(V_m)$. The solid line represents the result of a linear regression analysis. Over the

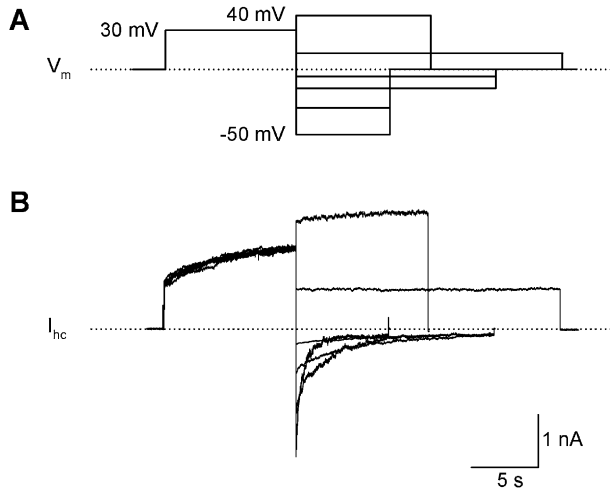

Fig. 2. Voltage dependence of the hemichannel currents. (*A*) Biphasic pulse protocol consisting of a constant depolarizing prepulse from 0 to 30 mV for 10 s, followed by a variable test pulse in the hyperpolarizing (−50, −30, −15, −5 mV) and depolarizing direction (15 and 40 mV) for 7 to 20 s. *Dotted line*: $V_m = 0$ mV. (*B*) Superimposed hemichannel currents, I_{hc}, associated with the pulse protocol. The pre-pulse resulted in an outward current that increased slowly with time. The hyperpolarizing test pulses gave rise to inward currents that deactivated incompletely with time. The depolarizing test pulses led to outward currents with virtually no time dependence. *Dotted line*: zero-current level.

voltage range examined, $g_{j,inst}$ showed a linear relationship with a moderate negative slope (zero V_m intercept: 0.98; slope = −0.01/mV). The correlation between $g_{j,inst}$ and V_m was significant statistically (regression coefficient $r = 0.6$; $P < 0.025$).

As shown in Fig. 4*B*, the function $g_{hc,ss} = f(V_m)$ was sigmoidal with a maximum at positive V_m and a minimum at negative V_m. The latter was distinctly different from zero, consistent with the view that most channels altered from the main state to the residual state, while few remained in the main state (Valiunas, 2002). The transition of $g_{hc,ss}$ from maximum to minimum occurred between about −40 and 40 mV. The smooth curve represents the best fit of data to the Boltzmann equation

$$\frac{g_{hc,ss}}{g_{hc,inst}} = \frac{g_{hc,max} - g_{hc,min}}{1 + e^{[-A(V_m - V_{m,0})]}} + g_{hc,min} \quad (1)$$

where $g_{hc,max}$ and $g_{hc,min}$ are the maximal and minimal conductances at large positive and negative V_m, respectively. $V_{hc,0}$ corresponds to V_m at which $g_{hc,ss}$ is half-maximally activated. A is a constant expressing gating charge $zq(kT)^{-1}$ (z: unitary positive charges q moving through the electric field applied; k: Boltzmann constant; T: temperature in Kelvin; *cf.* Harris, Spray & Bennett, 1981). The analysis yielded the following values: $V_{hc,0} = -1.08$ mV; $g_{hc,max} = 1.04$, $g_{hc,min} = 0.08$; $z = 4.0$. The function $g_{hc,ss} = f(V_m)$ reflects the gating behavior of Cx45 hemichannels and hence is relevant for the operation of Cx45 gap

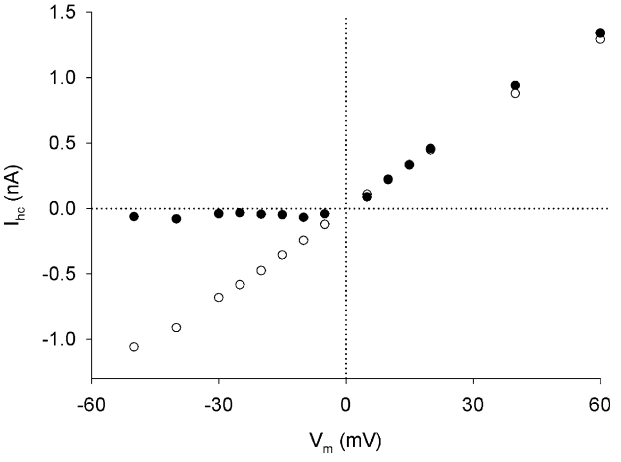

Fig. 3. Relationship between the hemichannel current, I_{hc}, and the membrane potential, V_m. Current signals I_{hc} gained at different V_m were analyzed to determine the amplitude of the instantaneous current, $I_{hc,inst}$, and the steady-state current, $I_{hc,ss}$. The symbols correspond to single determinations and were taken from a single experiment. (○): plot of $I_{hc,inst}$ as a function of V_m; and (●): plot of $I_{hc,ss}$ as a function of V_m. The function $I_{hc,inst} = f(V_m)$ was nearly linear. The function $I_{hc,ss} = f(V_m)$ exhibited a sharp break around $V_m = 0$ mV.

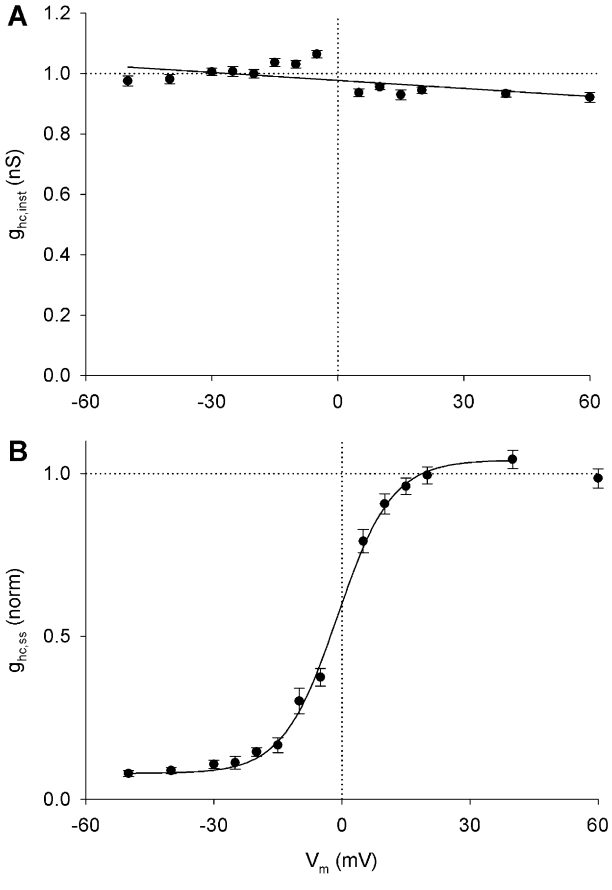

Fig. 4. Dependence of the hemichannel conductance, g_{hc}, on the membrane potential, V_m. The values of normalized $g_{hc,inst}$ and $g_{hc,ss}$ determined at different V_m were gathered from 8 cells, averaged and plotted as a function of V_m. The symbols correspond to mean values ±1 SEM. (*A*) The function $g_{hc,inst} = f(V_m)$ was linear and exhibited a small negative slope. The solid line represents the result of a linear regression analysis. The correlation between $g_{j,inst}$ and V_m was statistically significant (regression coefficient $r = 0.6$; $P < 0.025$). (*B*) The function $g_{hc,ss} = f(V_m)$ was sigmoidal. The smooth curve represents the best fit of data to the Boltzmann equation ($V_{hc,0} = -1.1$ mV; $g_{hc,min} = 0.08$; $z = 4.0$). For details, *see* text.

junction channels (*cf.* Elenes et al., 2001). The value of g_{hc} at $V_m = 60$ mV did not fit unequivocally into the set of data points. Hence, it was omitted from the curve-fitting procedure. Conceivably, it reflects an unspecific effect of Cx45 hemichannels and/or the contribution of an unknown current system.

Deactivation of Hemichannel Currents

The current signals elicited by the bipolar-pulse protocol were also used to study the kinetics of I_{hc} deactivation (Fig. 5*A*). Figure 5*B* shows selected current records obtained at a test potential of −20, −40 and −50 mV (from top to bottom). They indicate that I_{hc} deactivated faster when V_m was made more negative (*see* also Fig. 2). For analysis, the I_{hc} signals were subjected to a least-square curve-fitting procedure. It turned out that I_{hc} deactivation proceeded with a mono-exponential time course. The smooth curves superimposed on the current traces correspond to the best fit of data to the equation

$$I_{hc}(t) = (I_{hc,inst} - I_{hc,ss}) \cdot e^{-\left(\frac{t}{\tau_d}\right)} + I_{hc,ss} \quad (2)$$

where τ_d is the time constant of I_{hc} deactivation. The analysis of the records yielded the following values: $\tau_d = 6.7$, 1.5 and 0.9 s.

Figure 6 summarizes the τ_d data gathered from 8 cells. The values of τ_d were determined from individual I_{hc} records, averaged and plotted as a function of V_m. The graph includes data from current signals with a monotonic change in time. This was the case for voltages ranging from −50 to 5 mV. At $V_m >$ 5 mV, the records showed outward currents with no detectable decay or an inconsistent behavior, such as a small sustained or transient increase. Hence they were excluded from the analysis. Over the voltage range considered, τ_d increased progressively as V_m was made more positive. The smooth curve corresponds to the best fit of data to the exponential

$$\tau_d = \tau_{d,0} \cdot e(V_m/V_\tau), \quad (3)$$

where $\tau_{d,0}$ is the zero V_m intercept and V_τ the decay constant. The analysis yielded the following values: $\tau_{d,0} = 7.6$ s, and $V_\tau = 19.7$ mV.

Activation of I_{hc}

Figure 7*A* illustrates the pulse protocol adopted to explore the activation of I_{hc}. Starting from a V_h of

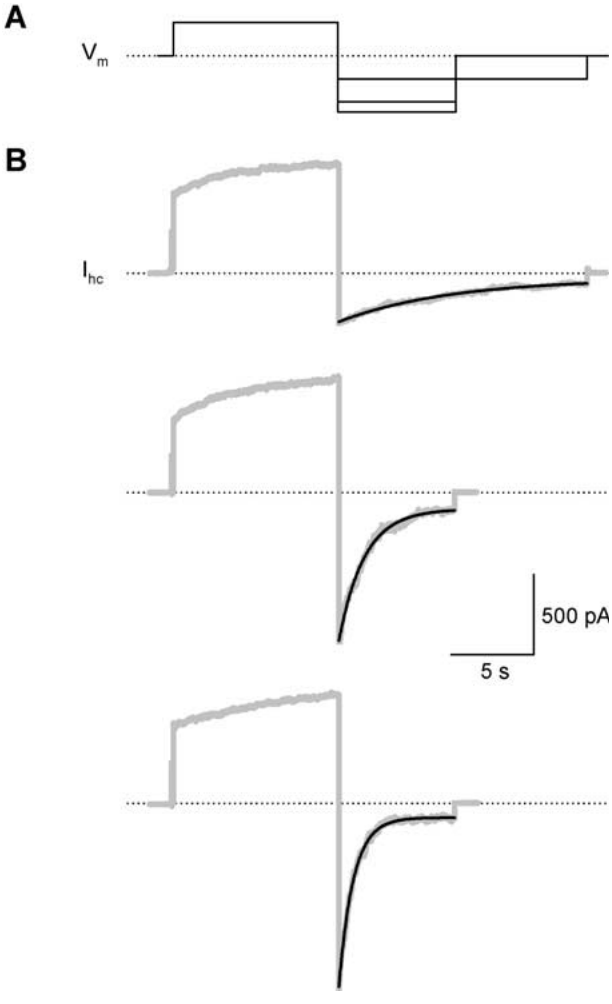

Fig. 5. Deactivation of hemichannel currents, I_{hc}. (*A*) Biphasic pulse protocol with a constant pre-pulse followed by a test pulse of different amplitude. (*B*) Family of I_{hc} records. The pre-pulse to V_m = 30 mV fully activated I_{hc}. The subsequent test pulse to V_m = −20, −40 and −50 mV revealed I_{hc} signals undergoing progressively faster deactivation (*gray traces*, from top to bottom). The smooth curves superimposed on the current records correspond to the best fit of data to a single exponential (*black traces*). V_m = −20 mV: τ_d = 6.7 s; V_m = −40 mV: τ_d = 1.5 s; V_m = −50 mV: τ_d = 0.9 s. *Dotted line*: zero-current level.

0 mV, V_m was first depolarized to 30 mV for 10 s and then hyperpolarized to −50 mV for 8 s. This provoked an outward current that activated maximally, followed by an inward current that deactivated maximally. Subsequently, V_m was returned to different levels for 30 s. The return potential permitted I_{hc} to activate with time. To visualize this process, a test pulse of 5 ms duration to −50 mV was delivered repetitively at progressively increasing time intervals. The test pulses were kept short to minimize an interference from I_{hc} deactivation. In these experiments, the current signals were digitized at 5 instead of 3.33 kHz.

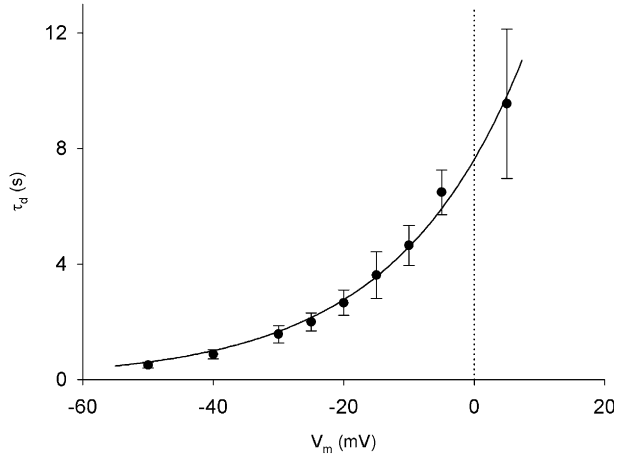

Fig. 6. Relationship between the time constant of I_{hc} deactivation, τ_d, and the membrane potential, V_m. The symbols correspond to mean values ± 1 SEM (n = 8). The graph shows that τ_d increased as V_m was made less negative. The smooth curve represents the best fit of data to a single exponential (for parameters, *see* text).

Figure 7*B* shows a continuous current record obtained at a return potential of 15 mV. This initiated the process of I_{hc} activation. On the one hand, this is visible as a time-dependent increase of the outward current (continuous trace interrupted by short current spikes) indicating a progressive activation of the channels. On the other hand, this is discernible as a pulse-to-pulse increase of the inward current spikes elicited by the short test pulses (envelope method). The spike amplitude eventually reached at steady state reflects the number of channels in the main state plus the number of channels in the residual state at V_m = 15 mV. Figure 7*C* illustrates the analysis of the current spikes elicited by the test pulses. The procedure utilized involved the following steps. To determine the initial amplitude of I_{hc}, the current segment over the first millisecond was discarded because of the limited response time of the recording set-up. The remaining segment was extrapolated linearly to the time t = 0 s, which indicated the beginning of the activation process. The values of $I_{hc,inst}$ obtained were then plotted as a function of time (●). The graph shows that I_{hc} increased with time. The smooth curve represents the best fit of data to the sum of two exponentials:

$$I_{hc}(t) = I_{hc}(0) + C_1\left[1 - e^{-\left(\frac{t}{\tau_{a1}}\right)}\right] + C_2\left[1 - e^{-\left(\frac{t}{\tau_{a2}}\right)}\right]. \quad (4)$$

$I_{hc}(0)$ is the current at time t = 0 s and corresponds to $I_{hc,min}$ associated with the hyperpolarizing pulse; τ_{a1} and τ_{a2} are the time constants of activation. The parameters C_1 and C_2 signify the respective amplitudes of I_{hc} at steady state and correspond to the

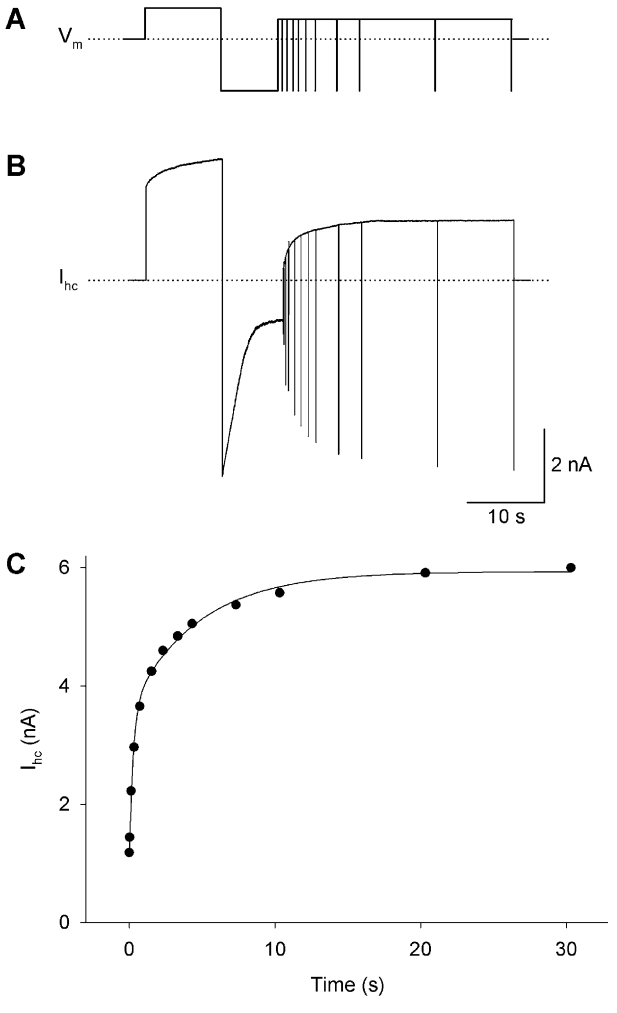

Fig. 7. Activation of hemichannel currents, I_{hc}. (*A*) Voltage protocol. A pre-pulse (V_m: 30 mV, duration: 10 s) was followed by a conditioning pulse (V_m: −50 mV; duration: 8 s) and a return pulse (V_m: 15 mV; duration: 30 s). During the latter, a test pulse (V_m, −50 mV; duration: 5 ms) was delivered repetitively at increasing time intervals. *Dotted line*: V_m = 0 mV. (*B*) Associated current trace. The pre-pulse served to fully activate I_{hc}. The conditioning pulse resulted in a maximal deactivation of I_{hc}. The return pulse allowed I_{hc} to activate. The test pulses gave rise to inward current surges of increasing amplitude, reflecting the activation process. *Dotted line*: zero-current level. (*C*) Plot of the amplitude of $I_{hc,inst}$ of the inward current surges as a function of time after initiation of I_{hc} activation. The symbols correspond to single determinations. The smooth curve represents the best fit of data to a double exponential. Time constants of I_{hc} activation: τ_{a1} = 0.42 s, τ_{a2} = 4.3 s.

contribution of the two processes. The analysis yielded the following values: τ_{a1} = 0.42 s and τ_{a2} = 4.3 s, C_1 = 2.4 nA and C_2 = 2.3 nA. To analyze the current directly associated with the return potential, the outward current trace interrupted by the short current spikes was subjected to a least-square curve-fitting procedure. The best fit was obtained with the sum of two exponentials for the following time constants: τ_{a1} = 0.38 s and τ_{a2} = 4.0 s. Hence, these values are comparable to those gained with the envelope method.

In an independent series of experiments, the two procedures of determining τ_a were applied sequentially rather than simultaneously. A comparison of the results revealed no systematic differences. For example, at a return potential of 30 mV, the respective time constants were as follows (envelope method/curve fitting procedure): τ_{a1} = 0.46/0.53 s and τ_{a2} = 4.4/4.8 s. The similarity of data gained with the two procedures suggests that the envelope method, in conjunction with the criteria chosen, is reliable to study the kinetics of I_{hc} activation. Since it allows more accurate measurements at V_m close to the reversal potential, it has been used for further experiments.

To elucidate the voltage sensitivity of I_{hc} activation, a series of experiments was performed stepping the return potential to different levels, i.e., −40, −30, −20, −15, −10, −5, 5, 10, 15, 20, 30 and 50 mV. At each return potential, the values of $I_{hc,inst}$ elicited by the test pulses were determined, normalized with respect to $I_{hc,inst}$ associated with the hyperpolarizing pre-pulse, and the respective conductances calculated. The normalized values of $g_{hc,inst}$ were then sampled, averaged and plotted as a function of time. The graph in Fig. 8 illustrates the results from 4 complete experiments. For clarity, it includes the data for selected voltages only, i.e., V_m = −30, −15, −5, 5, 15 and 30 mV (from bottom to top). It indicates that g_{hc} activated in a voltage-dependent manner. The activation was faster and less complete at more negative V_m, and slower and more complete at more positive V_m. At voltages negative to −15 mV, the data were best fitted by a single exponential giving rise to τ_{a1}, and at more positive voltages, by the sum of two exponentials giving rise to τ_{a1} and τ_{a2}. The smooth curves represent the best result of the curve fitting.

The time constants derived from the data presented in Fig. 8 and others from the same experiments were then used to establish the voltage dependence of τ_{a1} and τ_{a2}. Figure 9*A* shows the resulting plots of the functions $\tau_{a1} = f(V_m)$ (●) and $\tau_{a2} = f(V_m)$ (○), which characterize the fast and slow process of activation, respectively. It indicates that the two functions differ with respect to values and voltage sensitivity. On the one hand, τ_{a1} was maximal at $V_m \cong -20$ mV and declined more strongly at positive voltage than at negative voltage. On the other hand, τ_{a2} was maximal at $V_m \cong 15$ mV and decayed more prominently at negative voltage than at positive voltage. Furthermore, over the voltage range that yielded useful results, the values of τ_{a1} were smaller than those of τ_{a2}. Interestingly, a comparison of Figs. 6 and 9*A* indicates that there is no correspondence between the τ_d data and the τ_{a1} or τ_{a2} data.

The parameters C_1 and C_2 gained from the analysis were used to establish the relationships

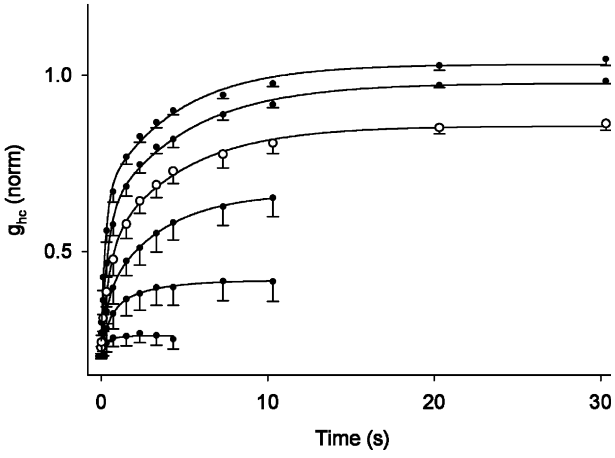

Fig. 8. Voltage dependence of g_{hc} activation. The activation of g_{hc} was explored with the envelope method (for details, *see* text). The data collected were sampled, averaged and plotted as a function of time. The results depicted were obtained at V_m = −30, −15, −5, 5, 15 and 30 mV (from bottom to top). The symbols correspond to mean values ± 1 SEM (n = 4). To emphasize the early phase of activation, the data at V_m = 5 mV are represented by the open circles. The smooth curves correspond to the best fit of data to the sum of two exponentials.

$C_1 = f(V_m)$ (●) and $C_2 = f(V_m)$ (○), which characterize the contribution of the fast and slow activation process at steady state, respectively. Figure 9*B* shows the resulting plots. The smooth curves represent the best fit of data to the Boltzmann equation

$$C = \frac{C_{max}}{1 + e^{\left[-A(V_m - V_{m,0})\right]}}. \quad (5)$$

C_{max} is the maximal C at positive V_m and $V_{m,0}$ corresponds to the voltage at which C is half-maximal (for further explanations, *see* Eq. 1). The analysis yielded the following parameters: fast process, $V_{m,0}$ = 3.2 mV, $C_{1,max}$ = 0.50, z = 2.0; slow process, $V_{m,0}$ = −9.6 mV, $C_{2,max}$ = 0.37, z = 6.8. Considering the values of $C_{1,max}$ and $C_{2,max}$, the maximal contribution of the fast and slow process amounts to 58 and 42%, respectively. A comparison of the two curves indicates that the two functions also differ with respect to values and voltage sensitivity. The fast process (●) was less voltage sensitive, operated over a broader V_m range and contributed a larger maximal amount. The slow process (○) was more voltage sensitive, operated over a narrower V_m range and contributed a smaller maximal amount.

Discussion

The results indicate that mouse Cx45 hemichannels expressed in human HeLa cells open up under appropriate experimental conditions, i.e., low $[Ca^{2+}]_o$ and a depolarized V_m. This is consistent with a recent

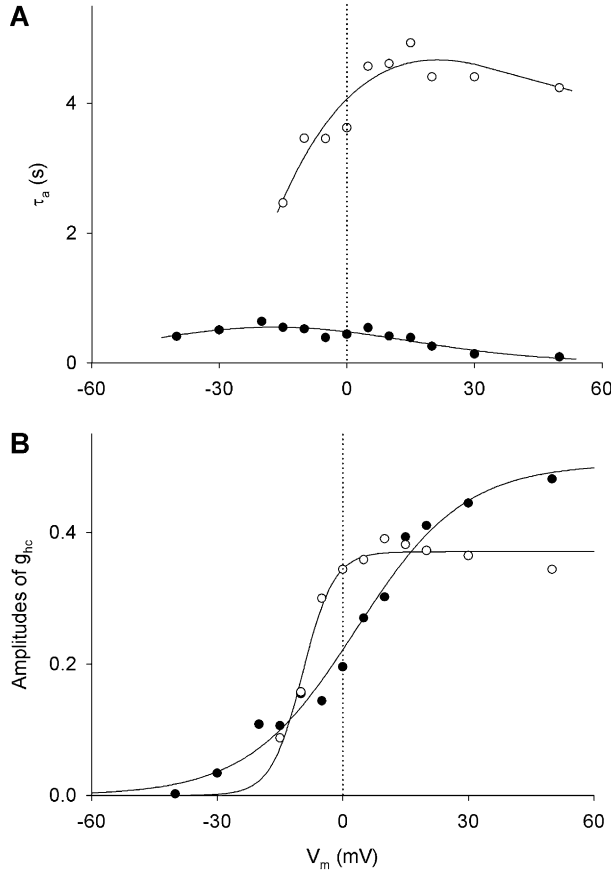

Fig. 9. Kinetic properties of I_{hc} activation. (*A*) Relationship between the time constants of I_{hc} activation, τ_a, and voltage, V_m. The time constants τ_{a1} (●) and τ_{a2} (○) characterize the fast and slow activation process, respectively. The curves were drawn by eye. (*B*) Relationship between the amplitudes of the activation processes at steady state and voltage, V_m. The parameters C_1 (●) and C_2 (○) characterize the contribution of the fast and slow process at steady state, respectively. The smooth curves correspond to the best fit of data to a Boltzmann equation, giving rise to the following values (C_1 data/C_2 data): $V_{m,0}$ = 3.2/−9.6 mV, C_{max} = 0.50/0.37, z = 2.0/6.8. For details, *see* text.

study of mCx45 (m: mouse) and cCx45 (c: chicken) hemichannels expressed in HeLa and RIN cells, respectively (Valiunas, 2002). The recruitment of operational hemichannels occurred in a $[Ca^{2+}]_o$-dependent manner (Bader, Weingart, Egger; *unpublished observations*) and was reversible. A concentration of 10 nM was adequate. It opened a maximal number of channels, preserved the basic properties of the cell membrane and kept the cells alive.

Voltage Dependence of Hemichannel Currents

A biphasic pulse protocol was used to examine the properties of Cx45 hemichannel currents, I_{hc}. The constant conditioning pulse served to activate the channels and the variable test pulse, to establish a

driving force of different amplitude and either polarity. This enabled us to study the conductive and kinetic properties of I_{hc}. The analysis of $I_{hc,inst}$, the current at the onset of the test pulse, yielded a linear function $g_{hc,inst} = f(V_m)$ with a negative slope significantly different from zero (*see* Fig. 4*A*). Assuming that $g_{hc,inst}$ does not involve channel gating (Vogel & Weingart, 1998), $g_{hc,inst} = f(V_m)$ is expected to reflect the sum of the conductance of single hemichannels in the main open state, $\gamma_{hc,main}$, i.e., $g_{hc,inst} = n \cdot \gamma_{hc,main}$ (*n*: number of channels). Hence, the function $g_{hc,inst} = f(V_m)$ is expected to resemble the relationship $\gamma_{hc,main\ state} = f(V_m)$. Indeed, it has been reported that $\gamma_{j,main\ state}$ exhibits a negative slope giving rise to larger values at negative V_m and smaller ones at positive V_m (Valiunas, 2002).

Are there other factors that may influence the function $g_{hc,inst} = f(V_m)$? HeLa cells exhibit two types of inward rectifying K^+ channels, one being voltage-dependent and Ca^{2+}-insensitive (Sauvé, Roy & Payet, 1983), the other one, voltage-independent and Ca^{2+}-sensitive (Sauvé et al., 1986; Díaz & Sepúlveda, 1995), and a volume-activated Cl^- current (Sahebgharani et al., 2001). Interference from these channels was minimized by adding channel blockers to the solutions (*see* Materials and Methods; *see* also Valiunas & Weingart, 2000). However, their contribution cannot be excluded completely. Another possibility is the limiting frequency response of the recording setup. However, the precautions taken to minimize this problem render it unlikely: use of low-resistance pipettes, coating of the pipette tips, use of a capacity-compensation circuit and curve-fitting with back extrapolation to determine $I_{hc,inst}$.

The analysis of $I_{hc,ss}$, the current at the end of the test pulse, revealed a sigmoidal function $g_{hc,ss} = f(V_m)$ with a maximum at positive V_m and a minimum at negative V_m (*see* Fig. 4). The best fit of data to the Boltzmann equation yielded the following values: $V_{m,0} = -1$ mV, $g_{hc,max} = 1.04$, $g_{hc,min} = 0.08$, $z = 4.0$. Several conclusions emerge from this relationship, (i) The decay of $g_{hc,ss}$ at negative V_m suggests that gap junction channels made of mCx45 hemichannels are gating with a negative polarity. (ii) The decay of $g_{hc,ss}$ from maximum to minimum occurred over a voltage range of about 80 mV. This is consistent with the behavior of Cx45 gap junction channels if one assumes that half of the transjunctional voltage drops across each hemichannel (*cf.* Vogel & Weingart, 1998). (iii) The $g_{hc,ss}$ did not decline to zero at large negative V_m. According to the general concept of gap junction channel behavior (*see*, e.g., Valiunas et al., 1999), this suggests that the Cx45 hemichannels switched from the main state to the residual state. However, this concept may need modification, since it has been found that few Cx45 hemichannels remain in the open position at large negative V_m (Valiunas, 2002). (iv) The function $g_{hc,ss} = f(V_m)$ crossed the zero-voltage axis at $g_{hc,ss} = 0.60$, indicating that a significant fraction of hemichannels dwelled in the residual state under this condition. This suggests that a similar fraction of Cx45 gap junction channels is in the residual state at $V_j = 0$ mV as well. Indeed, it has been reported that not all of these channels are open at $V_j = 0$ mV (Moreno et al., 1995; *see* also Elenes et al., 2001). However, the fraction of open channels is considerably larger than predicted from our data on Cx45 hemichannels. Hence, the voltage sensitivity of the hemichannels may be altered by the docking process (*cf.* Valiunas & Weingart, 2000). (v) The $g_{hc,ss}$ reached a maximum at $V_m \cong 40$ mV but moderately declined at more positive voltages. This may be due to a contribution from other channels (*see* above). (vi) The function $g_{hc,ss} = f(V_m)$ reached a minimum at $V_m \cong -40$ mV. This and the sensitivity to extracellular Ca^{2+} (*see* Recruitment of Hemichannels) render it unlikely that solitary Cx45 hemichannels are open in cardiac myocytes under physiological conditions (V_m: -60 to -90 mV).

A similar relationship $g_{hc,ss} = f(V_m)$ has been reported recently for mCx45 hemichannels ($V_{m,0} = 11.1$ mV, $g_{hc,max} = 2.34$, $g_{hc,min} = 0.21$, $z = 1.7$; Valiunas, 2002). However, this study revealed a more positive $V_{m,0}$ and a constant $g_{hc,max}$ at large positive V_m. These differences may reflect the different ionic solutions used (K^+ aspartate$^-$ versus KCl). The ratio $g_{hc,min}/g_{hc,max}$ was comparable in their and our studies (0.09 versus 0.08), while *z* was smaller in theirs (1.7 versus 4.0). The high voltage sensitivity of mCx45 hemichannels is consistent with that seen in mCx45 gap junction channels (Barrio et al., 1997; Elenes et al., 2001).

Kinetics of Hemichannel Currents

The current signals gained with the bipolar pulse protocol revealed that I_{hc} deactivation is governed by V_m. The time-dependent decay of I_{hc} followed a single exponential giving rise to the time constants τd (*see* Fig. 5). The values of τ_d increased progressively as V_m was made less negative, i.e., the less negative V_m, the slower was the deactivation of I_{hc}. The analysis of the τ_d data led to an exponential function $\tau_d = f(V_m)$ (*see* Fig. 6). The curve-fitting procedure yielded the following parameters: $\tau_{d,0} = 7.6$ s (zero V_m intercept); $V_\tau = -19.7$ mV (decay constant). Stepping V_m from -50 to 5 mV gave rise to a 19-fold increase in τ_d. Because of inconsistent current signals, τ_d could not be determined at $V_m > 5$ mV.

The kinetics of I_{hc} activation were examined with the envelope method using trains of short test pulses. The data collected indicate that g_{hc} activated in a voltage-dependent manner (*see* Fig. 8). The activation was faster but less complete at negative V_m and slower but more complete at positive V_m. At voltages

negative to −15 mV, the data were best approximated by a single exponential, but at −15 mV and more positive voltages, by the sum of two exponentials. With regard to the time course of activation, the voltage sensitivity of the time constants τ_{a1} and τ_{a2} was largely different (*see* Fig. 9*A*). The function $\tau_{a1} = f(V_m)$ was shallow (●) and yielded a maximum of ~0.6 s at around $V_m = -20$ mV. It declined partially at more negative V_m and more completely at more positive V_m. In contrast, the function $\tau_{a2} = f(V_m)$ was steep (○) and showed a maximum of ~4.9 s at around $V_m = 15$ mV. It decreased sharply at more negative V_m and moderately at more positive V_m. Hence, the functions $\tau_{a1} = f(V_m)$ and $\tau_{a2} = f(V_m)$ characterize a fast and slow process of activation, respectively. With regard to the extent of activation, the voltage sensitivity of the fast and slow process, i.e., $C_1 = f(V_m)$ and $C_2 = f(V_m)$, respectively, was distinctly different. At $V_m = 40$ mV, i.e., the most positive voltage that yielded reliable data, C_1 and C_2 both approached a maximum, i.e., $C_{1,max}$ and $C_{2,max}$. Under this condition, $C_{1,max}$ was larger than $C_{2,max}$. The respective contributions were 58 and 42%, respectively. Moreover, the function $C_1 = f(V_m)$ was less voltage-sensitive than the function $C_2 = f(V_m)$ ($C1$ data/C_2 data): $V_{m,0} = 3.2/-9.6$ mV; $z = 2.0/6.8$ (*see* Eq. 5 and legend to Fig. 9). Furthermore, the values of C_1 and C_2 at $V_m = 0$ mV were 0.20 and 0.34, respectively. This supports the view that a sizable fraction of hemichannels is not in the open state at $V_m = 0$ mV (*see* Fig. 9*B*). This is consistent with the finding that at $V_m = 0$ mV, $g_{hc,ss}$ is substantially different from $g_{hc,max}$ (*see* Fig. 4; *see* also Voltage Dependence of Hemichannel Currents).

It is generally accepted that gap junction channels and hemichannels exhibit two prominent conductance states that obey the scheme 'main state ⇔ residual state' (*cf.* Vogel & Weingart, 1998). Moreover, it has been proposed that changes in g_{hc} are due to reversible first-order processes whose forward and backward rates are unique functions of voltage (Harris et al., 1981). Therefore, the current change at a given voltage is expected to proceed with the same rate, irrespective of the voltage from which the process begins. This means that the time constants τ_d and τ_a ought to describe a unique function $\tau = f(V_m)$. However, our results indicate that this is not the case. It turned out that I_{hc} activation exhibits two time constants giving rise to $\tau_{a1} = f(V_m)$ and $\tau_{a2} = f(V_m)$. Neither of these functions represents a subset of $\tau_d = f(V_m)$ (*compare* Figs. 6 and 9*A*). For example, at $V_m = -30$ mV, a condition where τ_d and τ_{a1} are defined, $\tau_d = 1.7$ s and $\tau_{a1} = 0.64$ s; or at $V_m = -5$ mV, a condition where τ_d, τ_{a1} and τ_{a2} are defined, $\tau_d = 6.5$ s, $\tau_{a1} = 0.39$ s and $\tau_{a2} = 3.5$ s.

The time constants of hemichannel deactivation and activation, i.e., $\tau_{hc,d}$ and $\tau_{hc,a}$, correspond to the time constants of gap junction channel inactivation and recovery, i.e., $\tau_{j,i}$ and $\tau_{j,r}$. This convention has to be kept in mind in the following discussion. A first question to be discussed is: can the kinetics of I_{hc} deactivation explain the kinetics of I_j inactivation? A comparison of Cx45 hemichannel and gap junction channel data indicates that I_{hc} deactivates with a single time constant at each voltage examined, i.e., $\tau_{hc,d}$, while I_j inactivates with a single time constant at small voltages, i.e., $\tau_{j,i1}$, and two time constants at large voltages, i.e., $\tau_{j,i1}$ and $\tau_{j,i2}$ (*cf.* Barrio et al., 1997; Bader et al., 2003; but *see* also Moreno et al., 1995). The latter may reflect concomitant gating of both hemichannels of a gap junction channel (Banach & Weingart, 2000). However, data comparison indicates that the values of $\tau_{hc,d}$ are inconsistent with those of $\tau_{j,i1}$, despite the assumption that half of the transjunctional voltage is sensed by each hemichannel. Specifically, $\tau_{hc,d} < \tau_{j,i1}$ for a transjunctional voltage $V_j < 40$ mV and $\tau_{hc,d} > \tau_{j,i}$ for a $V_j > 40$ mV. This discrepancy suggests that hemichannel docking modifies the voltage sensitivity of the hemichannels. Another explanation may be that deactivation of a hemichannel and inactivation of a gap junction channel provoke a different voltage profile. While the former senses the entire voltage drop, the latter senses the voltage drop across two hemichannels in series, i.e., one that undergoes gating and hence switches from the open to the residual state, and one that remains in the open state.

Another question to be discussed is: what is the relationship between the kinetics of I_{hc} activation and the kinetics of I_j recovery? An exploratory study yielded results that contradict our results. Experiments performed on injected single oocytes expressing rat Cx46 or chicken Cx56 yielded a reasonable agreement between the time course of I_{hc} activation and I_j recovery determined at a single voltage, i.e., $V_m = 100$ mV (Ebihara et al. 1995). As outlined above, we failed to establish such a correlation. The reason for this discrepancy is unclear. A possibility is that the similarity of the time course of I_{hc} activation and I_{hc} recovery was unique to the voltage examined. Interestingly, experiments performed on pairs of hamster ventricular cells yielded a different result (Wang et al., 1992). These authors reported that $\tau_{j,i}$ was different from $\tau_{j,r}$ ($V_j = 80$ mV: $\tau_{j,i} = 430$ ms; $\tau_{j,r} = 300$ ms), a finding that is consistent with our observations on Cx45 hemichannels.

In conclusion, deactivation and activation of Cx45 hemichannels are best described by a single exponential and the sum of two single exponentials, respectively. Moreover, the time constants of the two processes do not coincide in a voltage plot. This suggests that activation and deactivation do not follow a simple reversible reaction scheme governed by first-order voltage-dependent processes. Hence, the formalism proposed for gap junction channels in amphibian blastomeres (Harris et al., 1981) has to be

extended to include more than two channel states. Such a model may then account for the time-dependent conductance changes of hemichannels and gap junction channels consisting of Cx45 and other connexins.

Biological Significance

It is generally thought that gap junction hemichannels are silent structures that serve as precursors to establish gap junction channels. This notion assumes that they acquire their functional role only after docking with each other. However, recent findings indicate that this concept may need revision. There is evidence that Cx43 gap junction hemichannels in ventricular myocytes open up in the presence of low extracellular Ca^{2+} or during metabolic inhibition (Kondo et al., 2000). These observations complement earlier reports that elevated cytoplasmic Ca^{2+} (Rose & Loewenstein, 1976; Noma & Tsuboi, 1987) or reduced ATP^{2-} (Sugiura et al., 1990) affect the transfer properties of gap junction channels (for further references, *see* Harris, 2001). The relevance of these regulatory mechanisms of hemichannels may be that metabolically impaired cells take up Ca^{2+} via hemichannels and thereby enhance functional uncoupling from adjacent cells, i.e., ATP^{2-} depletion may open up hemichannels and force gap junction channels to close. This would provide a metabolic strategy to separate healthy cells from injured cells and hence save energy. Such a mechanism may be crucial during cellular insults, the outcome being dependent on the ATP^{2-} and Ca^{2+}-sensitivity of the connexins.

In the context of cardiac electrophysiology, the regulatory role of Ca^{2+} and ATP^{2-} on gap junction channels and hemichannels may have the following potential impact. The opening of hemichannels brought about by reducing $[Ca^{2+}]_o$ and/or $[ATP^{2-}]_i$ leads to an increase in g_{hc}. This increase in membrane conductance short-circuits the excitatory inward current of the action potentials, thereby impairing dV_m/dt_{max}, the maximal upstroke velocity of action potential (*cf*. Kléber et al, 2004). This in turn leads to a decrease in conduction velocity of the electrical impulse, θ. Likewise, the closing of gap junction channels brought about by elevating $[Ca^{2+}]_i$ and/or reducing $[ATP^{2-}]_i$ leads to a decrease in g_j and thereby decreases θ. Since changes in dV_m/dt_{max} or g_j act independently and synergistically on θ, small changes have already sizable effects on θ. The ionic and metabolic requirements that lead to such detrimental effects prevail during cardiac ischemia (*cf*. Kléber et al, 2004) and hence are relevant for many disease circumstances.

These considerations provoke the following generalized picture. Under physiological conditions, gap junction channels are usually open, while hemichannels are closed. Conversely, under pathophysiological condition, hemichannels open up, while gap junction channels close.

We thank D. Lüthi for expert technical assistance and H. Imboden, Department of Cell Biology, University of Bern for valuable discussions. The cells were provided by K. Willecke, Institute of Genetics, University of Bonn, Germany. This work was supported by the Swiss National Science Foundation (31-55297.98 and 31-67230.01 to R.W.).

References

Bader, P., Desplantez, T., Weingart, R. 2003. Kinetic properties of currents carried by mCx45 gap junction channels and hemichannels. *In:* Proceedings of the 2003 International Gap Junction Conference, p 41. Cambridge, UK, August 23–28, 2003

Bader, P., Weingart, R. 2003. Conductive and kinetic properties of connexin45 hemichannels. *Pfluegers Arch.* **445:**R69

Banach, K., Weingart, R. 2000. Voltage gating of Cx43 gap junction channels involves fast and slow current transitions. *Pfluegers Arch.* **439:**248–250

Barrio, L.C., Capel, J., Jarillo, J.A., Castro, C., Revilla, A. 1997. Species-specific voltage-gating properties of connexin−45 junctions expressed in *Xenopus* oocytes. *Biophys. J.* **73:**757–769

Bruzzone, R., White, T.W., Paul, D.L. 1996. Connections with connexins: the molecular basis of direct intercellular signalling. *Eur. J. Biochem.* **238:**1–27

Bukauskas, F.F., Weingart, R. 1994. Voltage-dependent gating of single gap junction channels in an insect cell line. *Biophys. J.* **67:**613–625

Butterweck, A., Gergs, U., Elfgang, C., Willecke, K., Traub, O. 1994. Immunochemical characterization of the gap junction protein connexin45 in mouse kidney and transfected human HeLa cells. *J. Membrane Biol.* **141:**247–256

De Vries, S.H., Schwartz, E.A. 1992. Hemi-gap junction channels in solitary horizontal cells of the catfish retina. *J. Physiol.* **445:**201–230

Díaz, M., Sepúlveda, F.V. 1995. Characterisation of Ca^{2+}-dependent inwardly rectifying K^+ currents in HeLa cells. *Pfluegers Arch.* **430:**168–180

Ebihara, L., Berthoud, V.M., Beyer, E.G. 1995. Distinct behavior of connexin56 and connexin46 gap junction channels can be predicted from the behavior of their hemi-gap-junctional channels. *Biophys. J.* **68:**1796–1803

Elenes, S., Martinez, A.D., Delmar, M., Beyer, E.C., Moreno, A.P. 2001. Heterotypic docking of Cx43 and Cx45 connexons blocks fast voltage gating of Cx43. *Biophys. J.* **81:**1406–1418

Elfgang, C., Eckert, R., Lichtenberg-Fraté, H., Butterweck, A., Traub, O., Klein, R.A., Hülser, D.F., Willecke, K. 1995. Specific permeability and selective formation of gap junction channels in connexin-transfected HeLa cells. *J. Cell. Biol.* **129:**805–817

Gros, D., Jongsma, H.J. 1996. Connexins in mammalian heart function. *Bioessays.* **18:**719–730

Harris, A.L. 2001. Emerging issues of connexin channels: biophysics fills the gap. *Quart. Rev. Biophys.* **34:**325–472

Harris, A.L., Spray, D.C., Bennett, M.V.L. 1981. Kinetic properties of a voltage-dependent junctional conductance. *J. Gen. Physiol.* **77:**95–117

Kondo, R.P., Wang, S.-Y., John, S.A., Weiss, J.N., Goldhaber, J.I. 2000. Metabolic inhibition activates a non-selective current through connexin-hemichannels in isolated ventricular myocytes. *J. Mol. Cell. Cardiol.* **32:**1859–1872

Kléber, A.G., Rudy, Y. 2004. Basic mechanisms of cardiac impulse propagation and associated arrhythmias. *Physiol. Rev.* **84:**431–488

Li, H., Liu, T.F., Lazrak, A., Peracchia, C., Goldberg, G.S., Lampe, P.D., Johnson, R.G. 1996. Properties and regulation of gap junction hemichannels in the plasma membranes of cultured cells. *J. Cell Biol.* **134:**1019–1030

Martin, P.E., Blundell, G., Ahmad, S., Errington, R.J., Evans, W.H. 2001. Multiple pathways in the trafficking and assembly of connexin 26, 32 and 43 into gap junction intercellular communication channels. *J. Cell Sci.* **114:**3845–3855

Moreno, A.P., Laing, J.G., Beyer, E.G., Spray, D.C. 1995. Properties of gap junction channels formed of connexin 45 endogenously expressed in human hepatoma (SKHep1) cells. *Am. J. Physiol.* **268:**C356–C365

Nilius, B., Prenen, J., Voets, T., Eggermont, J., Droogmans, G. 1998. Activation of volume-regulated chloride currents by reduction of intracellular ionic strength in bovine endothelial cells. *J. Physiol.* **506.2:**353–361

Noma, A., Tsuboi, N. 1987. Dependence of junctional conductance on proton, calcium and magnesium ions in cardiac paired cells of guinea-pig. *J. Physiol.* **382:**193–211

Rose, B., Loewenstein, W.R. 1976. Permeability of a cell junction and the local cytoplasmic free ionized calcium concentration: A study with aequorin. *J. Membrane Biol.* **28:**87–119

Sahebgharani, M., Hardy, S.P., Lloid, A.W., Hunter, A.C., Allen, M.C. 2001. Volume-activated chloride currents in HeLa cells are blocked by Tamoxifen but not by a membrane impermeant quaternary analogue. *Cell. Physiol. Biochem.* **11:**99–104

Sauvé, R., Roy, G., Payet, D. 1983. Single channel K^+ currents from HeLa cells. *J. Membrane Biol* **74:**41–49

Sauvé, R., Simoneau, C., Monette, R., Roy, G. 1986. Single-channel analysis of the potassium permeability in HeLa cancer cells: Evidence for a calcium-activated potassium channel of small unitary conductance. *J. Membrane Biol* **92:**269–282

Severs, N.J., Rothery, S., Dupont, E., Coppen, S.R., Yeh, H.-I., Ko, Y.-S., Matsushita, T., Kaba, R., Halliday, D. 2001. Immunocytochemical analysis of connexin expression in the healthy and diseased cardiovascular system. *Microsc. Res. Tech.* **52:**301–322

Sugiura, H., Toyama, J., Tsuboi, N., Kamiya, K., Kodama, I. 1990. ATP directly affects junctional conductance between paired ventricular myocytes isolated from guinea pig heart. *Circ. Res.* **66:**1095–1102

Trexler, E.B., Bennett, M.V.L., Bargiello, T.A., Verselis, V.K. 1996. Voltage gating and permeation in a gap junction hemichannel. *Proc. Natl. Acad. Sci. USA* **93:**5836–5841

Valiunas, V. 2002. Biophysical properties of connexin−45 gap junction hemichannels studied in vertebrate cells. *J. Gen. Physiol.* **119:**147–164

Valiunas, V., Weingart, R. 2000. Electrical properties of gap junction hemichannels identified in transfected HeLa cells. *Pfluegers Arch.* **440:**366–379

Valiunas, V., Manthey, D., Vogel, R., Willecke, K., Weingart, R. 1999. Biophysical properties of mouse connexin30 gap junction channels studied in transfected human HeLa cells. *J. Physiol.* **519.3:**631–644

Van Veen, T.A., Van Rijen, H.V., Jongsma, H.J. 2000. Electrical conductance of mouse connexin45 gap junction channels is modulated by phosphorylation. *Cardiovasc. Res.* **46:**496–510

Vogel, R., Weingart, R. 1998. Mathematical model of vertebrate gap junctions derived from electrical measurements on homotypic and heterotypic channels. *J. Physiol.* **510.1:**177–189

Wang, H.-Z., Li, J., Lemanski, L.F., Veenstra, R.D. 1992. Gating of mammalian cardiac gap junction channels by transjunctional voltage. *Biophys. J.* **63:**139–151

Willecke, K., Eiberger, J., Degen, J., Eckhardt, D., Romualdi, A., Güldenagel, M., Deutsch, U., Söhl, G. 2002. Structural and functional diversity of connexin genes in the mouse and human genome. *Biol. Chem.* **383:**725–737